Neuron, Vol. 44, 651–661, November 18, 2004, Copyright ©2004 by Cell Press

Axon Branch Removal at Developing Synapses by Axosome Shedding

Derron L. Bishop,[2,3,4] Thomas Misgeld,[1,2,3] Mark K. Walsh,[2,5] Wen-Biao Gan,[2,6] and Jeff W. Lichtman[1,2,*]
[1]Department of Molecular and Cellular Biology
Harvard University
7 Divinity Avenue
Cambridge, Massachusetts 02138
[2]Department of Anatomy and Neurobiology
Washington University School of Medicine
St. Louis, Missouri 63110

Summary

In many parts of the developing nervous system, the number of axonal inputs to each postsynaptic cell is dramatically reduced. This synapse elimination has been extensively studied at the neuromuscular junction, but how axons are lost is unknown. Here, we combine time-lapse imaging of fluorescently labeled axons and serial electron microscopy to show that axons at neuromuscular junctions are removed by an unusual cellular mechanism. As axons disappear, they shed numerous membrane bound remnants. These "axosomes" contain a high density of synaptic organelles and are formed by engulfment of axon tips by Schwann cells. After this engulfment, the axosome's contents mix with the cytoplasm of the glial cell. Axosome shedding might underlie other forms of axon loss and may provide a pathway for interactions between axons and glia.

Introduction

In many parts of the developing nervous system, axonal branches that establish synapses in prenatal life are removed a short time later. This axon branch and synapse loss reduces the number of postsynaptic cells driven by a neuron and at the same time reduces the number of different neurons that provide innervation to each postsynaptic cell. For example, thalamic neurons in the retinogeniculate system lose approximately ten inputs for every one input that is maintained (Chen and Regehr, 2000). Similar input elimination occurs in the cerebellum (Lohof et al., 1996), in parasympathetic and sympathetic autonomic ganglia (Lichtman, 1977; Lichtman and Purves, 1980), and at neuromuscular junctions (Wyatt and Balice-Gordon, 2003). Because of the accessibility of the neuromuscular junction, naturally occurring synapse elimination has been studied most extensively here. Multiple motor neurons initially send branches that converge at each muscle fiber's synaptic site (Balice-Gordon and Lichtman, 1990; Brown et al., 1976; Colman et al., 1997; Redfern, 1970; Riley, 1981; Walsh and Lichtman, 2003). Within the first several postnatal weeks, however, all but one of the branches to each neuromuscular junction weaken and ultimately disappear (Colman et al., 1997). This loss of inputs to muscle fibers is explained by branch trimming rather than motor neuron death (Brown et al., 1976; Keller-Peck et al., 2001). The morphological correlates of input loss during synapse elimination are disconnected axons in the vicinity of neuromuscular junctions that sometimes end in enlarged tips. These swollen axon tips were called, suggestively, "retraction bulbs" (Balice-Gordon et al., 1993; Bixby, 1981; Korneliussen and Jansen, 1976; Riley, 1981). Recent time-lapse imaging has confirmed that these structures are the distal tips of axons that have been eliminated from neuromuscular junctions (Keller-Peck et al., 2001; Walsh and Lichtman, 2003). Still, the way in which these axon branches and their terminal bulbs are removed is not understood.

Several cellular mechanisms can account for how these axons disappear. The most popular idea is that axons retract (like a fishing line that is brought in), and axonal contents are shuttled to other axon branches (Riley, 1981), but axon retraction has not been directly documented at the neuromuscular junction. Alternatively, axons may undergo a classic Wallerian-type degeneration as suggested by some ultrastructural data (Rosenthal and Taraskevich, 1977). However, Wallerian degeneration normally removes an entire axon arbor rather than prunes a subset of an axon's branches, as occurs during synapse elimination. Mechanisms similar to Wallerian degeneration are involved in developmental axon removal in *Drosophila* (Watts et al., 2004), but the loss of inputs during mammalian synapse elimination appears to be mechanistically distinct (Gillingwater et al., 2003).

Alternatively, axons could be removed in a manner that combines features of both of the cellular mechanisms mentioned above. For example, the removal process could involve disto-proximal disintegration of the axon (similar to the shortening of a burning fuse). In this case, axonal fragments would be left behind as the axon appears to retract. Indeed, other cell types use such shedding to release excessive cellular contents (Denzer et al., 2000).

One way to better understand how axons are removed during development is to directly observe axon retraction using imaging techniques with better temporal and spatial resolution than previously available. With the development of transgenic mice that express variants of green fluorescent protein in their motor neurons, following synaptic rearrangements through time-lapse imaging has become feasible (Feng et al., 2000; Walsh and Lichtman, 2003). In this work, we use these mice to image axon removal over intervals of days, hours, minutes, and seconds. In addition, to obtain high-resolution information about the subcellular events underlying this

*Correspondence: jeff@mcb.harvard.edu
[3]These authors contributed equally to this work.
[4]Present address: E.F. Ball Medical Education Center, Ball State University, Muncie, Indiana 47306.
[5]Present address: Wilmer Ophthalmological Institute, Johns Hopkins University School of Medicine, Baltimore, Maryland 21287.
[6]Present address: Molecular Neurobiology Program, Skirball Institute, Department of Physiology and Neuroscience, New York University School of Medicine, New York, New York 10016.

dynamic process, we use correlated confocal and serial electron microscopy.

These approaches revealed that naturally occurring axon removal during development uses a previously unrecognized cellular mechanism. As axons retreat from neuromuscular junctions, they shed membrane-enclosed "axosomes" that are entirely contained within surrounding glia. This mechanism is clearly distinct from previously described forms of axonal degeneration and actually leads to the mixing of axonal and glial cytoplasm.

Results

Remnants of Retreating Axons at Developing Neuromuscular Junctions

Using transgenic mice that express fluorescent proteins in the cytoplasm of motor axons (see Experimental Procedures), we monitored junctions as they underwent the transition from multiple to single innervation. At neuromuscular junctions in the second postnatal week, fluorescence imaging showed three patterns: some neuromuscular junctions were contacted by two axons whose terminals were segregated to largely nonoverlapping regions (Gan and Lichtman, 1998), others were singly innervated with a second bulb-tipped axon nearby (Keller-Peck et al., 2001; Walsh and Lichtman, 2003), and the rest were singly innervated. Previous time-lapse imaging has indicated that neuromuscular junctions near such bulb-tipped axons had lost innervation from that axon within the previous day or two (Walsh and Lichtman, 2003).

We followed 34 retreating axons over several days. None of these bulb-tipped axons persisted for more than 48 hr. In some cases, the axon branch had entirely disappeared back to its origin on the parent axon between views. Often, we observed that the bulb was farther from the junction at the second view, implying that the terminal axon branch was not removed all at once, but rather in a distal to proximal order. Unexpectedly, we observed four cases (12%) in which fluorescent remnants of the removed axon were still present at the junction (Figure 1A). None of these fluorescent remnants persisted for more than 24 hr. Looking at several hundred neuromuscular junctions at this age, we noted two kinds of remnants: large spheres up to 10 μm in diameter near the junction (Figure 1A) and groups of smaller spherules along what may have been the original path of the axon (see below). Confocal reconstructions of bulb-tipped axons near singly innervated junctions revealed that in 72% of cases (18 of 25) such remnants could be seen.

To study the fate of these remnants with higher temporal resolution, we turned to acute explants of muscle where movement artifacts (such as those occurring due to respiration, pulse, and muscle movements) were minimized. We observed that larger remnants underwent shape changes and lost their fluorescence over several hours ($n = 6$; Figure 1B). The removal of these large remnants occurred in steps as they divided into progressively smaller pieces, each of which typically disappeared within several minutes (Figure 1C).

In several cases ($n = 5$), we directly observed how the large remnants originated from retreating axons. In the example shown in Figure 2A, a distal bulb and more proximal swollen part of the axon were connected by a thin axonal bridge (Figure 2A, inset in first frame), which disintegrated and thus left behind a large remnant (Figure 2A, asterisk). The disintegrating part of the bridge itself gave rise to a string of minute remnants along its original path (Figure 2A, inset in second frame). The more proximal part of the bridge, which was thicker, remained attached to the swollen axon segment. This feature, a swollen axonal segment with a protruding axonal process, was commonly seen in retreating axons (Figures 2A and 2B; see also Figure 1A and Figure 4). Eventually, such protrusions disappeared; in some cases they shortened and appeared to be reabsorbed into the more proximal axon, establishing a new terminal bulb. Although this shortening appears like axonal retraction, we typically saw minute remnants shed as the axons shortened (Figure 2B; see also Supplemental Movies S1, S2, and S4 and Supplemental Figures S1 and S2 at http://www.neuron.org/cgi/content/full/44/4/651/DC1/). How much axonal content is lost as opposed to shuttled back is not clear in all cases, but, in some situations at least, the vast majority of axonal shortening can be accounted for by remnant formation (Figure 2A and Supplemental Movie S3). Indeed, when we followed retreating bulb-tipped axons near synapses ($n = 15$) over time, we could see remnants in 87% of cases. Fewer remnants (23%; $n = 17$) were seen at greater distances from the neuromuscular junctions (Supplemental Figure S1 and Supplemental Movie S2).

The time-lapse images also provided insight into the mechanism that underlies remnant formation. Both large remnants (Figure 1C) and terminal bulbs (Figure 1B, last frame) underwent dramatic shape changes (>90%; $n = 67/70$). These shape changes were often caused by the formation of nonfluorescent fissures, which appeared and disappeared within seconds (Figure 3A; Supplemental Figure S2 and Supplemental Movies S4 and S5 at http://www.neuron.org/cgi/content/full/44/4/651/DC1/). While almost all of these fissures disappeared without discernible consequence, in some cases they engulfed small regions of the axon's cytoplasm, giving rise to new remnants (Figure 3B and Supplemental Movie S6). It is possible that these fissures are Schwann cell processes impinging the axon (see below). Indeed, cells surrounding bulb-tipped axons were immunoreactive for S100, a well-characterized marker of Schwann cells. Further evidence supporting glial involvement was that the small remnants underwent rapid movements within a constrained volume, most likely because they were inside Schwann cells (see Supplemental Movie S1).

Axosome Shedding as a Mechanism of Axon Removal

To confirm the identity of the processes impinging axon bulbs and to reveal the structure of the remnants, we imaged the same bulb with correlated light and serial electron microscopy (Figure 4A and Supplemental Movie S7 [http://www.neuron.org/cgi/content/full/44/4/651/DC1/]; see also Gan et al., 1999 and Experimental Procedures). Bulbs were easily recognized; they were entirely sheathed in Schwann cells, contained randomly ar-

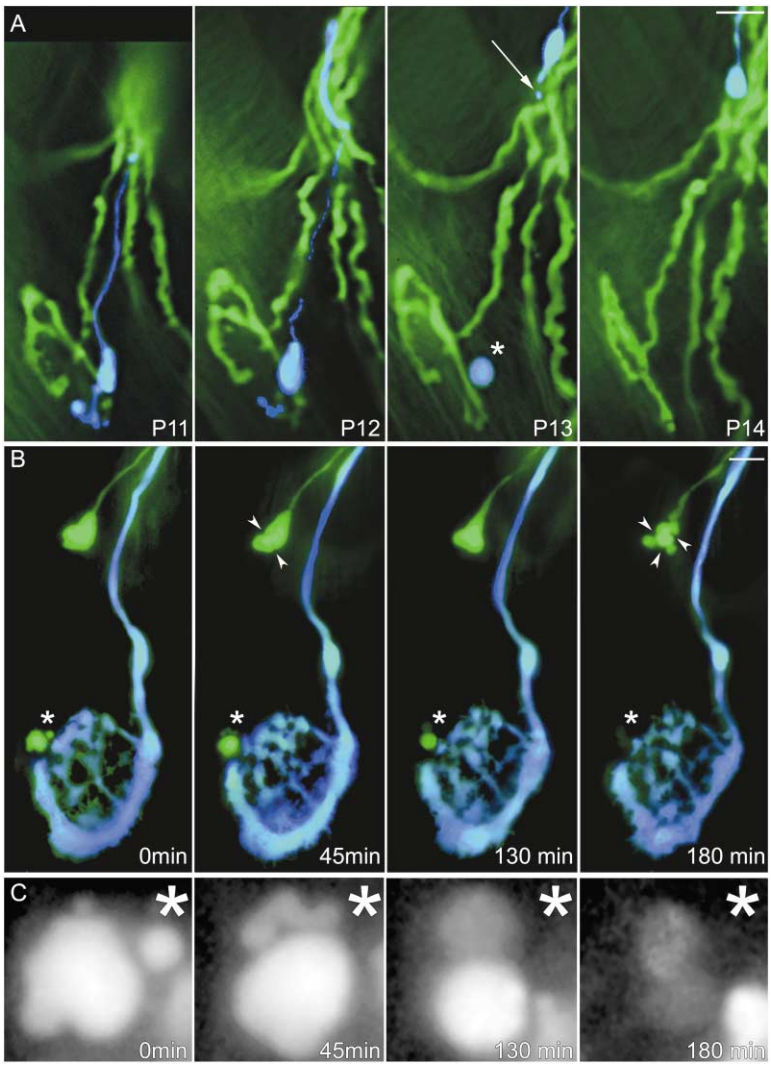

Figure 1. Axonal Remnants Associated with Axon Removal from Developing Neuromuscular Junctions

(A) In vivo time-lapse imaging of a neuromuscular junction innervated by two differentially labeled axons (see Experimental Procedures) at P11. The junction was followed for 3 days as one axon (blue) was removed. On P13, a large remnant of the blue axon (asterisk) remains at the junction, while the distal bulb of the blue axons is now ~50 μm away. Another smaller remnant (arrow) appears near a protrusion that extended from the bulb. The remnants are no longer visible 1 day later (P14). (B) A similar remnant (asterisk) can be seen in an explanted muscle at P9. Near a singly innervated junction (blue axon), a second green bulb-tipped axon is visible. The large remnant at the synapse changes shape over 2 hr and finally disappears 1 hr later. The bulb at the tip of the green axon also undergoes several changes in shape. Arrowheads show sites where fissures in the bulb appear. (C) Stepwise partitioning and dimming of the large remnant shown in (B) (grayscale image of green channel). Scale bar, 10 μm in (A) and (B); (C) is a 620% magnification of (B). High-resolution versions of figures and Supplemental Data can be downloaded at http://www.mcb.harvard.edu/Faculty/Lichtman.html.

ranged mitochondria, and possessed a high density of clear vesicles (Figure 4E). The vesicle's size (mean = 41.7 nm; SD = 4.9) and clear circular appearance resembled synaptic vesicles of age-matched singly innervated neuromuscular junctions (mean = 41.0 nm; SD = 4.6).

Surrounding most of the bulbs (n = 8/11), we found membrane bound spherical structures, ranging in size from 220 nm to 894 nm (n = 13), which, based on serial images, were not connected to the bulb (Figure 4). These structures, which we named "axosomes," contained the same organelles that were found in the bulb itself: clear vesicles and occasional mitochondria (Figures 4C–4E). The strong resemblance of the constituents of axosomes to that of bulbs argues that axosomes are derived from bulbs and hence are the remnants previously observed with fluorescence microscopy. Axosomes were completely enveloped by Schwann cell fingers and often were demarcated by both their own membrane and a second parallel membrane from the Schwann cell (Figures 4C–4E). In all but one case, the axosomes and their parental bulb showed no degenerative changes (like electron-dense cytoplasm or disrupted mitochondria), indicating that axosomes are not formed by Wallerian-type degeneration.

A considerable number of axosomes were so close to the bulb (<1 μm) that they would not be resolved as separate entities with fluorescence imaging. For example, in Figure 4, there were four membrane-enclosed vesicle-laden structures (diameter 300 nm) in the immediate vicinity of the axon's bulb. These ultrastructural data suggest that light microscopic time-lapse imaging might underestimate the extent to which axosome shedding contributes to axon removal. Electron microscopy also provided support for the idea that glial cells may be instrumental in the formation of axosomes. In addition to the four axosomes in Figure 4, there were three small vesicle-filled buds on the bulb that were each connected by narrow (150 nm) stalks. These putative "proto-axosomes" were surrounded by impinging Schwann cell fingers.

Axosome Shedding also Contributes to Synaptic Segregation

Axon branches that terminate in bulbs are found not only once synapse elimination is over, but also within multiply innervated junctions as competing axons segregate from each other (Gan and Lichtman, 1998). Bulbs

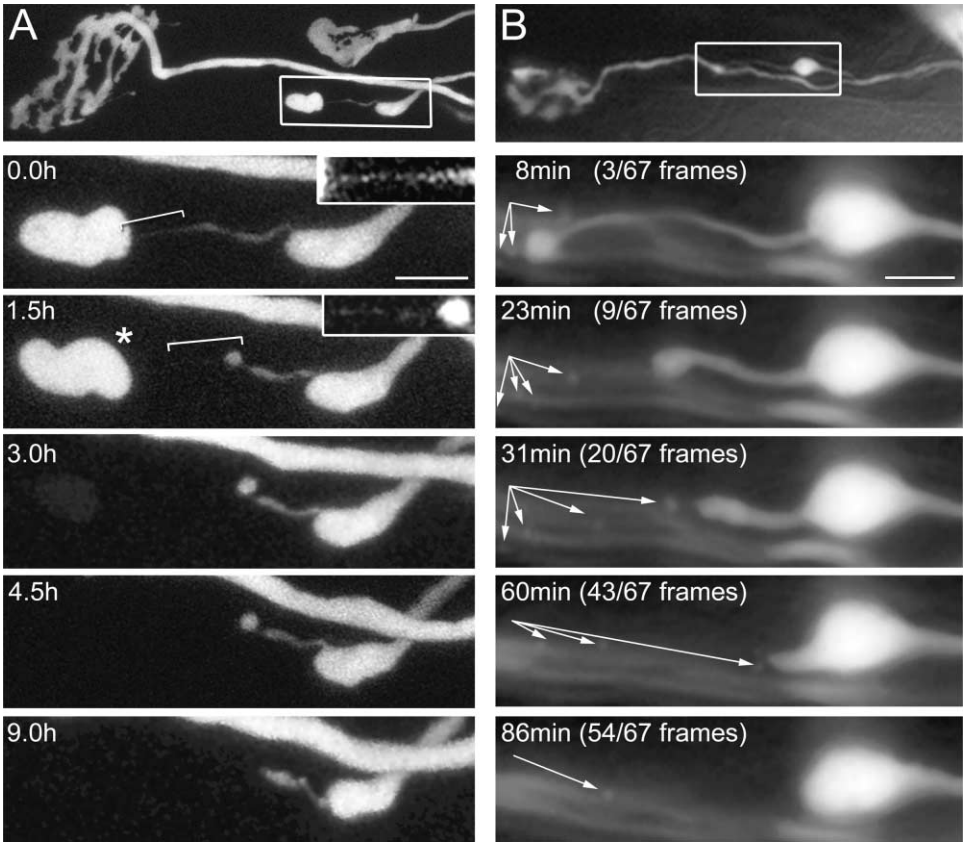

Figure 2. Remnant Formation from Bulb-Tipped Axons

(A) Confocal time-lapse series of an acute explant from a P12 mouse showing how disintegration of a thin axon bridge (marked by bracket in first frame, shown enlarged to 200% in inset) leads to both the formation of a large remnant (asterisk) and a trail of small remnants (area marked by bracket in second frame, shown enlarged in inset, 200%). The remainder of the bridge forms a protrusion on the more proximal axon swelling, while the remnants disappear. (B) In a P10 muscle, small remnants form as a protrusion from a bulb retracts (frames from Supplemental Movie S1 at http://www.neuron.org/cgi/content/full/44/4/651/DC1/). Scale bars, 5 μm in (A) and (B). Upper panel in each column shows lower-magnification view of retreating axon; the boxed area is shown at higher magnification in lower panels.

within junctions were similar to the terminal bulbs already described. For example, in Figure 5A (see also Supplemental Movie S8 at http://www.neuron.org/cgi/content/full/44/4/651/DC1/), the photoconverted branch of the green axon that extends into the blue axon's synaptic territory ended in a bulb that was lifted several micrometers from the surface of the muscle and entirely sheathed by a Schwann cell process. The bulb

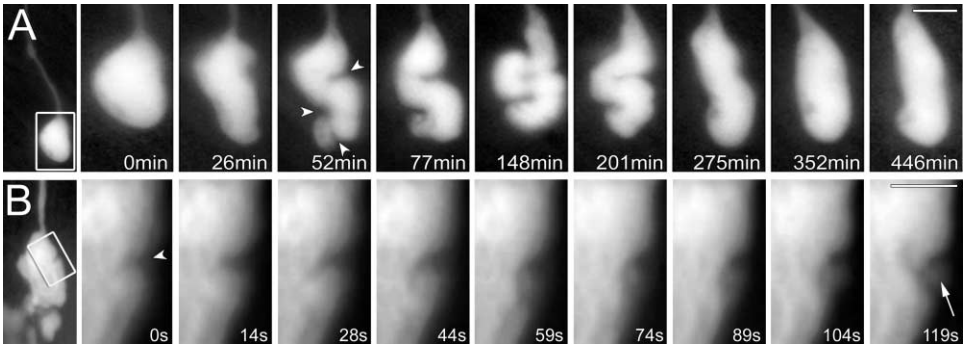

Figure 3. Rapid Changes in the Shape of Axonal Bulbs

(A) A bulb from an acute P8 explant undergoes bouts of deformation and quiescence over 7 hr. The shape changes were caused by nonfluorescent fingers that suddenly impinged the bulb's outer contour and formed fissures (arrowheads; frames from Supplemental Movie S5 at http://www.neuron.org/cgi/content/full/44/4/651/DC1/). (B) In some instances, these impingements (arrowhead) engulfed parts of an axonal bulb, giving rise to remnants (arrow; details of frames from Supplemental Movie S6). Scale bars, 2.5 μm in (A) and (B). Left panel in each row shows lower-magnification view of bulb; the boxed area is shown in higher magnification in time series.

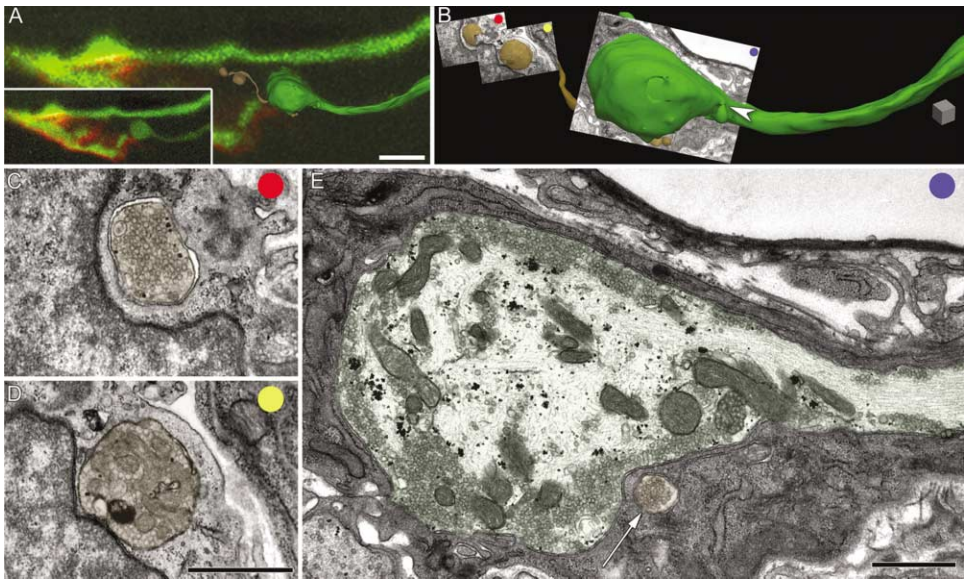

Figure 4. Double Membrane Bound Axosomes near Retreating Axons

(A) A surface rendering of a serial electron microscopic reconstruction of a bulb-tipped axon (green) superimposed on the confocal image of the same site (inset: confocal image alone; this junction was fixed with glutaraldehyde, hence the high autofluorescent background; postsynaptic acetylcholine receptors [red] are labeled by fluorescently tagged α-bungarotoxin). Several axonal remnants (brown) that surround the bulb were reconstructed from the electron micrographs. (B) Three electron micrographs (shown in [C], [D], and [E] below) intersect the bulb where these micrographs are located. Red, yellow, and blue circles have been inserted into the upper right corner of each micrograph for orientation. A "proto-axosome" can be seen to bud off the surface of the bulb (white arrowhead). (C–D) A glial cell surrounds the axosomes (pseudocolored brown), which contain vesicles and mitochondria. (E) The parent bulb (green) is laden with a high density of synaptic organelles with clusters of vesicles and mitochondria scattered within the bulb. A small axosome (brown; arrow) is separated from the parent bulb. Scale bars, 5 μm in (A), 1 μm in (B) (gray cube), 1 μm in (D)–(E) (scale bar in [D] also applies to [C]).

contained a dense accumulation of 40 nm (mean = 43.2 nm; SD = 5.1) vesicles in its distal tip and a large cluster of mitochondria (Figure 5B) near the thin axon stalk. Immediately adjacent ($<$1 μm) to the bulb, there were two axosomes embedded within Schwann cells (Figures 5A–5C). Although the bulb was photoconverted, no reaction product was found in axosomes, indicating that they were not attached to the bulb at the time of lipophilic dye labeling. Nonetheless, it is likely that these inclusions were at one time associated with the dye-labeled axon, because they were immediately adjacent to it and contained 40 nm vesicles (Figure 5C). Such vesicle-filled profiles were not observed in regions of the Schwann cell that were $>$2 μm from the retreating process. The most distal part of the bulb shown in Figure 5 appeared to be in the process of being engulfed (Figure 5D). A slender Schwann cell process had intercalated into a fissure in the bulb, leaving the proto-axosome attached by only a very thin ($<$100 nm) stalk. These observations suggest that axon branches of segregating terminals are removed in the same way that axons are completely removed from neuromuscular junctions later during the synapse elimination process.

Axonal Contents Are Transferred to Glial Cells

One consequence of axosome shedding would be the removal of vesicles from the retreating axons as they move farther from their former junctional sites. Indeed, we noted a dramatic difference between the axon bulbs based on their position in relation to synaptic sites. Bulbs far from neuromuscular junctions ($>$25 μm) contained fewer 40 nm vesicles (70.4 vesicles/μm^3 for bulb shown in Figure 6A) than bulbs near ($<$5 μm) neuromuscular junctions (1027 vesicles/μm^3 for the bulb shown in Figure 4E). Immunostaining for a vesicle-associated protein, synaptophysin, also showed evidence of vesicle loss associated with position, because bulbs and remnants at or close to synapses showed 2- to 3-fold higher levels of synaptophysin than those bulbs or remnants found in nerve fascicles ($n = 95$; $p < 0.001$ by Student's t test; Figure 6F).

Interestingly, analysis of the cytoskeleton within bulb-tipped axons provided evidence that the cytoskeletal structure of these axons is defective. First, microtubules were sparser than those in axons attached to neuromuscular junctions. In one bulb-tipped axon, microtubules were not visible at all. Second, neurofilaments always appeared to be highly disorganized within bulbs ($n = 11$; Figure 4E and Figure 6D) in sharp contrast to intact preterminal axons (Figure 4E and Figure 7B). In some instances, another area of disorganized neurofilaments was also found in retreating axons proximal to the disarray in the bulb (Figure 7C). The absence of microtubules (the main tract for fast anterograde and retrograde transport; Hirokawa et al., 1998) and the disarray of neurofilaments (a major cargo of slow axonal transport and potentially a linker to other cargo molecules) might indicate inhibited transport. Therefore, the difference in prevalence of synaptic organelles between bulbs near and away from synapses is explained by local shedding of axosomes and not caused by evacuation of synaptic organelles by retrograde transport.

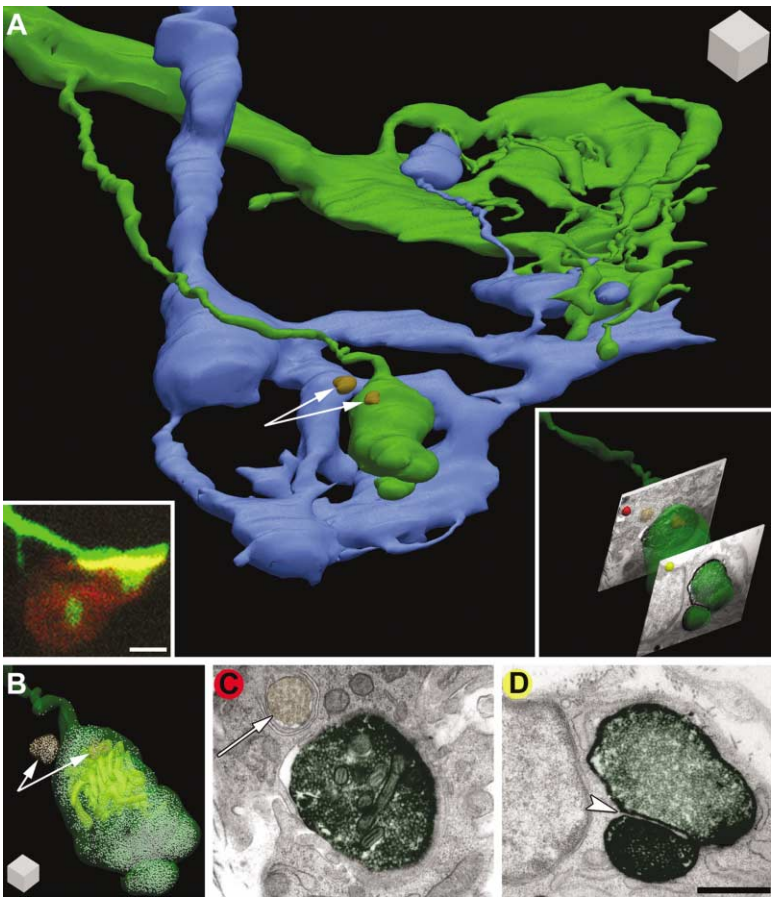

Figure 5. Axosome Shedding during Synaptic Segregation

(A) A surface rendering of the serial electron microscopic reconstruction of a highly segregated multiply innervated junction from a P7 mouse. The green axon was DiI labeled and photoconverted (left inset shows confocal image prior to photoconversion; DiI, green; acetylcholine receptors, red). The photoconversion product is visible as a dark precipitate in electron micrographs. Both axons have a bulb-tipped branch extending into the territory occupied by the competing input. Two axosomes (pseudocolored brown) near the green bulb are visible (arrows). Right inset shows the location of the micrographs shown in (C) and (D). (B) A semitransparent rendering showing the contents of the green axon's bulb and the two axosomes nearby (brown; arrows). The mitochondria (yellow) within the bulb are clustered near the proximal thin axon branch. The remainder of the bulb is filled with 40 nm vesicles. (C) Electron micrograph showing glial sheathing of axosome (arrow). (D) Electron micrograph showing the intrusion of a glial finger (arrowhead) into the base of a proto-axosome still connected to the bulb by a thin stalk. Scale bars, 1 μm in (A) (5 μm in left inset), 0.5 μm in (B) (gray cube), and 1 μm in (D) (scale bar in [D] also applies to [C]).

What is the ultimate fate of the shed axonal material? Close inspection of confocal reconstructions of axonal bulbs labeled with fluorescent proteins in some cases revealed a very weak fluorescent glow, which appeared to delineate a Schwann cell associated with the bulb (10%; $n = 11$ near 110 bulb-tipped axons; Figure 8). This fluorescence is most prominent in the nucleus of the Schwann cell as expected for cytoplasmic fluorescent protein, which can pass nucleopore complexes (Ribbeck and Gorlich, 2001), and is excluded from membrane bound organelles within the cytoplasm. Schwann cells that were not associated with axons in the process of being removed did not show such fluorescence (0.6%; $n = 1$ fluorescent Schwann cell at 171 singly innervated junctions; $p < 0.001$). This observation suggests that axosome material ultimately can become incorporated by the engulfing Schwann cell.

Discussion

Historically, there have been two competing models to explain axon removal during developmental synapse elimination: axon fragmentation akin to Wallerian degeneration (Rosenthal and Taraskevich, 1977) and axon retraction (Bixby, 1981; Riley, 1981). While some forms of developmental axon removal in flies can be explained by a degenerative process, which resembles Wallerian degeneration (i.e., fast fragmentation of axon branches; Watts et al., 2004), the known mechanisms do not account for naturally occurring axon removal in mammals. We chose to study this phenomenon at the developing neuromuscular junction, as new tools have become available to study cellular phenomena with better spatial and temporal resolution. Our observations revealed an unexpected mechanism (Supplemental Figure S3 at http://www.neuron.org/cgi/content/full/44/4/651/DC1/). Axosome shedding appears to constitute a different means of axon removal, in which axonal material is released into surrounding glial cells. We speculate that intermixing of axonal and glial cytoplasm could serve as a signal between neurons and glia.

The shedding of axonal material and the formation of axosomes has to our knowledge not been described previously. Many cell types, however, use shedding of membrane bound material to accomplish important metabolic and signaling functions. For example, megakaryocytes form platelets by shedding the tips of long cellular protrusions known as "proplatelets" (Italiano and Shivdasani, 2003). Intriguingly, rings of microtubules form within proplatelets before they are shed, similar to ring-like microtubular structures described in retracting axons in vitro (He et al., 2002) and in "budding" synaptic boutons at the *Drosophila* neuromuscular junction (Roos et al., 2000). However, axosomes did not contain major microtubular assemblies, and retreating axons were largely devoid of microtubular tracks (which is also true for axons undergoing disassembly in *Drosophila*; Watts et al., 2003, 2004). Another example of

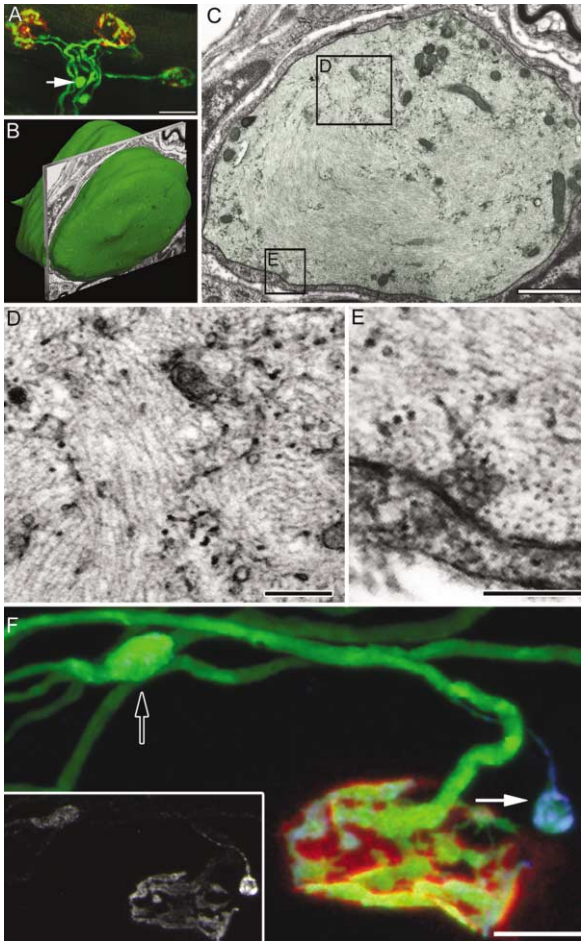

Figure 6. Organelle Content and Cytoskeleton Structure Change as Axons Retreat from Neuromuscular Junctions

(A) A confocal image of a bulb (arrow) that is in a nerve fascicle more than 25 μm from neuromuscular junction sites. (B) A surface rendering of a serial electron microscopic reconstruction of the bulb indicated by the arrow in (A) with a single electron micrograph intersecting it, which is shown in (C). (C) The bulb (green) contains few 40 nm vesicles and is sheathed by Schwann cell processes. (D) Localized neurofilament disorganization in axonal bulb (position of micrograph is outlined by the upper box in (C). Similar neurofilament disorganization can be found in the bulb in Figure 4E. (E) Six 40 nm vesicles clustered near the membrane of the bulb. Such vesicles are rare in bulbs far away from synapses (position of the micrograph is outlined by the bottom box in [C]). (F) Confocal image showing higher levels of synaptophysin immunoreactivity (blue) in a bulb that is close to a neuromuscular junction (white arrow) than in a bulb that is farther away (black arrow) from this or any other synapse (inset shows synaptophysin staining alone). Scale bars, 25 μm in (A); 1 μm in (C); 0.25 μm in (D) and (E); 10 μm in (F).

shedding in bone marrow-derived cells is the formation of "exosomes," small (50–100 nm) membrane bound vesicles released by a wide variety of blood and immune cells, including reticulocytes, platelets, B and T lymphocytes, and dendritic cells (Denzer et al., 2000). In reticulocytes, exosomes serve mainly to remove undesired membrane proteins like the transferrin receptor during erythrocyte maturation. However, exosome-like particles appear to also have a major signaling function, not only between immune cells, but also during *Drosophila* development, where they are known as "argosomes" (Greco et al., 2001). While platelets and exosomes are shed into the extracellular space, argosomes are taken up by neighboring cells by "trans-endocytosis." In cell culture systems, similar ephrin-based signaling mechanisms involving rac-dependent trans-endocytosis appear to mediate cellular retraction (Marston et al., 2003). While exosomes in the immune system are known to form through multivesicular bodies (a feature absent in retreating axons at the neuromuscular junction), the ultrastructural correlate of argosome formation is unresolved. An important question for future study of axosomes will be to clarify their relationship to other forms of shed exovesicles during development. Recently, ultrastructural examination of synapses in the hippocampus (Spacek and Harris, 2004) revealed that axons and dendrites extend small protrusions into neighboring neurons and glial cells. Some of these "spinules" appear to finally end as double membrane bound inclusions in the recipient cell due to trans-endocytosis. It has been suggested that spinules are involved in regulating synaptic competition in the CNS (Spacek and Harris, 2004), so axosome-like structures perhaps not only play a role during synaptic competition in the PNS, but similar mechanisms could be of importance in the CNS. Remarkably, numerous double membrane bound structures are seen in the developing cerebellum (Eckenhoff and Pysh, 1979), where climbing fibers undergo large-scale synapse elimination (Lohof et al., 1996).

Axosomes do not appear to be formed by the established mechanisms of exovesicle shedding, which require either tubulin loops (platelets; Italiano and Shivdasani, 2003), multivesicular bodies (exosomes; Denzer et al., 2000), or clathrin-coated pits (trans-endocytosis; Spacek and Harris, 2004). So how do they form?

In principle, axosome formation could be cell autonomous. Alternatively, the active participation of another cell type could be required. Wallerian degeneration is the classical example of axon-autonomous disintegration, with subsequent phagocytosis of remnants by scavenging glial cells and macrophages (Hirata and Kawabuchi, 2002). Similar mechanisms govern the removal of cell remnants after apoptosis (Henson et al., 2001), although more active roles for phagocytic cells have been suggested (Conradt, 2002). During axon pruning in invertebrate systems, the mechanism appears to be similar to Wallerian degeneration (Watts et al., 2003). The participation of glial cells in this process has been demonstrated recently, but whether they actively dismantle axons or whether they play a "scavenger" role (as they do in classical Wallerian degeneration) is not entirely clear (Awasaki and Ito, 2004; Broadie, 2004; Watts et al., 2004). However, axosomes are morphologically distinct from axonal fragments during Wallerian-type degeneration (Gillingwater et al., 2003). Further, synapse elimination and axonal pruning at the neuromuscular junction proceed normally in WLD-S mice, where Wallerian degeneration is severely delayed (Gillingwater and Ribchester, 2001). Considering that glial cells completely surround highly dynamic intact bulbs and small glial cell fingers intercalate into nascent axosomes, it appears likely that glial cells are actively involved. In addition, glial cells may actively help to maintain axons (Lin et

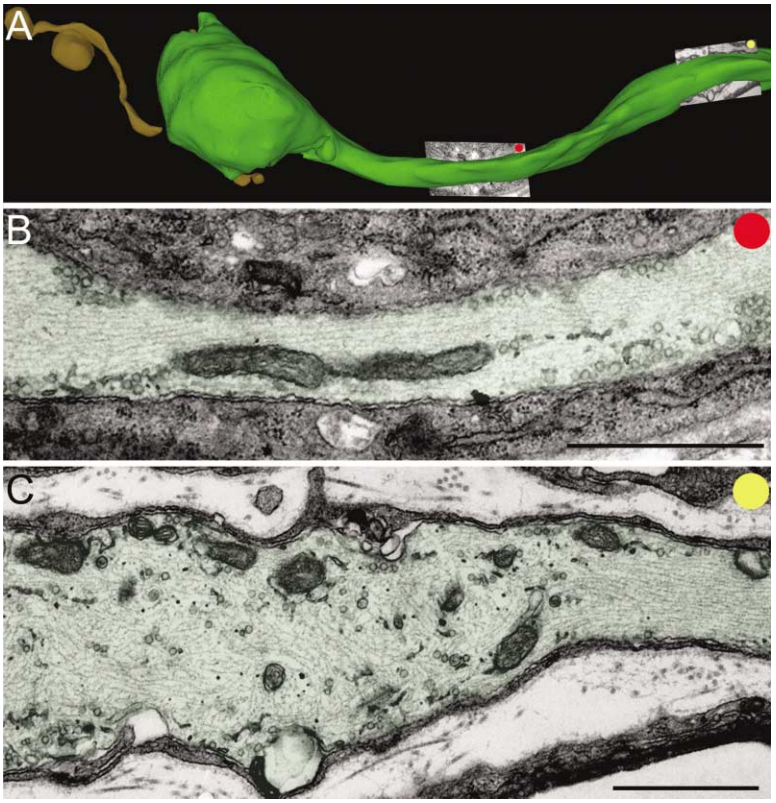

Figure 7. Neurofilament Disorganization Prior to Bulb Formation

(A) A surface rendering of a retreating axon (same as Figure 4) has two electron micrographs inserted proximal to the bulb. A red and yellow circle appears in the upper right corner for orientation. (B) The distal electron micrograph through the axon (green) shows two mitochondria, a few vesicles, and ordered neurofilaments. (C) The proximal electron micrograph through the axon (green) shows a transition between ordered and disorganized neurofilaments. The neurofilaments are disorganized both in the swollen axon segment (shown here) and the more distal bulb that tips this axon (see Figure 4E; also 6D for another example of disorganized neurofilaments in a bulb). Scale bars, 0.5 μm in (B) and (C).

al., 2000; Reddy et al., 2003), but whether this function is disrupted during synapse elimination is not known.

We can only speculate at this time on the functional significance of axosome formation. Considering that axosomes are fully enclosed within glial cells, their detachment and eventual dissolution would prevent the uncontrolled release of cellular contents into the extracellular space, thus mitigating an immune response. This is especially important in light of the fact that, in some parts of the brain, the majority of axons are lost during development and that throughout life the nervous system enjoys an immune-privileged status (Wekerle et al., 1986), where certain antigens remain sequestered. This same strategy of cellular containment is used during programmed cell death, where apoptosis allows for controlled removal of large numbers of cells without the detrimental effects of necrotic cell death (Henson et al., 2001). In addition, axosomes themselves could serve as signaling particles in the same way that exosomes and argosomes do (Denzer et al., 2000; Greco et al., 2001).

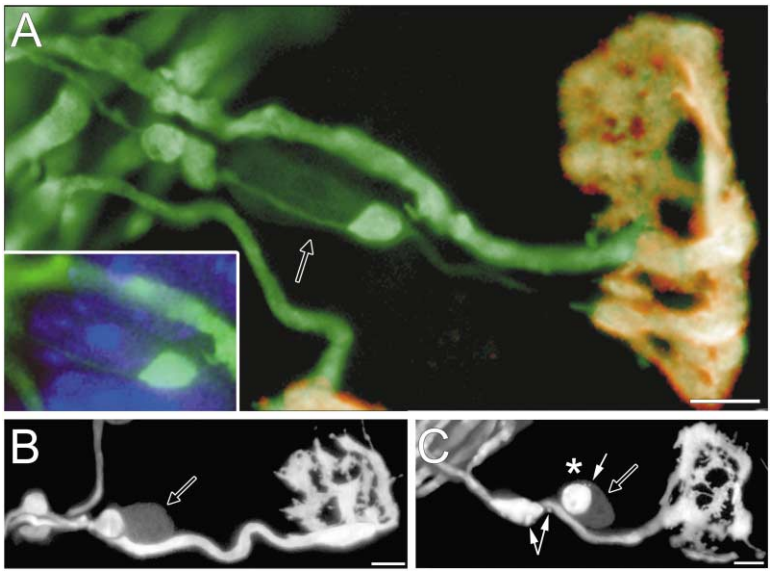

Figure 8. Axosome Shedding Leads to Mixing of Axonal and Glial Cytoplasm

(A) Confocal image of a bulb-tipped axon near a synapse. A thin axon stretch connects the distal bulb with a proximal swelling. A weakly fluorescent Schwann cell (black arrow) with a process protruding toward the synapse can be seen adjacent to the bulb. Inset shows nuclear stain (blue) with DAPI. (B) and (C) show other examples of glial cells labeled by transfer of axonal cytoplasm. In (B), the Schwann cell caps the axonal bulb. In (C), a large remnant (asterisk) is seen inside the labeled Schwann cell (black arrow), and smaller axosomes are seen near the bulb and the remnant (white arrows). Scale bars, 5 μm in all panels.

However, in these cases, the exovesicles in question largely carry cell membranes and little cytoplasm. Our results, in contrast, raise the interesting possibility that the signaling could be based on the admixture of the cytoplasm of the axon and the glial cell. This mechanism adds to the already well-described relationships between neurons and glia where trophic and synaptic intermediates are exchanged through extracellular release by one cell type followed by reuptake by the other (Nedergaard et al., 2003).

Regardless of the mechanism, the consequence of the signaling between the axosomes and glia may also serve as a key to understanding a number of puzzling observations about Schwann cells. For example, in our serial electron microscopic reconstructions, we often noticed that competing axons were sheathed by different Schwann cell tubes. However, only a single tube persists into adulthood. What is the fate of Schwann cells associated with the vacating axon? One possibility is that axosome-associated signaling serves as an indicator to the Schwann cell to migrate away or even undergo an apoptotic cell death (Nakao et al., 1997). In fact, neonatal terminal and preterminal Schwann cells undergo apoptosis in response to denervation (Trachtenberg and Thompson, 1996). Generally, Schwann cell death is believed to be due to loss of a survival signal. However, induction of cell death by exovesicles is a recognized mechanism in the immune system (Martinez-Lorenzo et al., 1999). Another curious feature of Schwann cells that have lost their associated axon in adults is that they release acetylcholine (Dennis and Miledi, 1974; Miledi and Slater, 1968). Currently, it is unclear how glial cells obtain the cellular machinery required for neurotransmitter release. Immune exosomes are known to transfer antigen-presenting capability to nonprofessional antigen-presenting cells (Denzer et al., 2000). In contrast to antigen presentation, neurotransmitter release requires a cytoplasmic apparatus, so axosome contents would have to gain access to glial cytoplasm. Cytoplasmic mixing could provide such materials.

Experimental Procedures

In Vivo Imaging

Double transgenic mice that expressed YFP in all motor axons (YFP-16 line) and CFP in a subset of motor axons (CFP-S) were used (Feng et al., 2000).

Briefly (for details, see Walsh and Lichtman, 2003), in vivo imaging techniques were utilized to allow for the repeated imaging (time intervals ranging from several hours to several days; pups recovered and returned to parents between views) of neuromuscular junctions in neonatal mice that were undergoing the process of synapse elimination. Previously described transgenic mice that express spectral variants of cytoplasmic GFP in subsets of motor neurons were used (Feng et al., 2000), thus providing a vital presynaptic label. Fluorescently conjugated α-bungarotoxin (Molecular Probes, Eugene, OR) was used as a postsynaptic label (3% of acetylcholine receptors were labeled). Images of individual junctions were taken using a standard epifluorescence microscope (Eclipse E800; Nikon, Melville, NY) with a cooled CCD camera (MicroMAX 512BFT; Roper Industries, Duluth, GA) and single and triple dichroic emission filters (Chroma Technology Corp., Brattleboro, VT). Exciting wavelengths were provided by a xenon lamp and rapidly switched exciting filters (Lambda DG-4; Sutter Instrument Co., Novato, CA; filters, Chroma). Stacks of images (1 μm steps) of individual junctions were obtained (piezoelectric objective Z axis stepper; Physik Instrumente, Waldbronn, Germany), from which two-dimensional images were derived by extracting in-focus information from each image plane to create image mosaics. Control experiments (Walsh and Lichtman, 2003) indicated that the dynamism that was witnessed in these studies was not induced by nerve damage, muscle damage, or photodamage. In a series of control experiments, triangularis sterni muscles from mice that expressed YFP in all motor axons were fixed without prior imaging. Confocal microscopy of these muscles confirmed the presence of fluorescent remnants near bulb-tipped axons, which appeared to have recently left a nearby neuromuscular junction (data not shown).

Ex Vivo Imaging in Muscle Explants

Neuromuscular explants were obtained from postnatal (P8–13) YFP-16 or YFP-16 $\times$ CFP-S transgenic animals. The triangularis sterni and its innervating nerves were dissected in Neurobasal A medium (Invitrogen, Carlsbad, CA) by bilateral paravertebral cuts and removal of the diaphragm and the intrathoracic organs. The tissue was pinned with 0.1 mm insect pins into a Sylgard-coated 3.5 cm dish. The tissue was kept on a heated (34°C–36°C) stage in oxygenated (95% O_2/5% CO_2) Neurobasal A medium (perfusion rate, 0.5–1.0 ml/min). In this way, muscles could be kept alive until Wallerian degeneration lead to fragmentation of motor axons after about 10–12 hr (Parson et al., 2004). The following observations exclude a contribution of Wallerian degeneration to axosome shedding in the explants: (1) most observations that are described here were made within the first 6 hr of explant preparation, well before Wallerian degeneration sets in—indeed, once the preparation neared the end of its lifetime, axosome shedding was rarely seen; (2) in this preparation, Wallerian degeneration leads to fast wholesale fragmentation of entire axons, of which we saw no evidence in our explants before 10–12 hr; (3) the intermediate stages of axosome shedding that we describe were all also seen in fixed, unimaged material.

Images were taken with a BX51WI microscope (Olympus, Melville, NY) equipped with a 20$\times$, 0.5 NA water or a 100$\times$, 1.0 NA water objective lens and a z stepper (Ludl Electronic Products, Hawthorne, NY) and with a SensiCam camera (The Cooke Corp., Auburn Hills, MI) controlled by MetaMorph software (Universal Imaging Cooperation, Molecular Devices, Downingtown, PA). Other time series were acquired on a BioRad confocal system (BioRad MRC-1024; Hercules, CA). Images were edited in Photoshop (Adobe, San Jose, CA). To obtain single planes from image stacks, in-focus information was manually extracted from each individual plane.

Immunostaining and Quantification of Synaptophysin Content

Triangularis sterni muscles from YFP-16 transgenic mice were dissected in Neurobasal A medium and fixed in 4% paraformaldehyde in phosphate-buffered saline (pH 7.4). Synaptophysin was detected using a polyclonal antiserum (1:500; Zymed, San Francisco, CA) and a Cy3-labeled donkey anti-mouse secondary antibody (1:1000; Molecular Probes). Immunostainings were scanned on a confocal microscope (BioRad MRC-1024) using a 60$\times$, 1.4 NA oil objective. Nuclei were counterstained with 4′,6-diamidino-2-phenylindole (DAPI; Sigma, St. Louis, MO) and imaged on a Zeiss Axioplan microscope with a 100$\times$, 1.4 NA oil objective lens. Maximum intensity projections were used to represent confocal stacks. To avoid obscuring cellular detail on some axons, in-focus information was manually extracted from individual planes, and mosaic images were created in Photoshop.

To estimate the content of synaptophysin in bulbs, images were taken on a BX51WI microscope (Olympus, Melville, NY) equipped with a SensiCam camera (The Cooke Corp., Auburn Hills, MI) and a 40$\times$, 1.15 NA water lens. Bulbs were delineated in the YFP channel, and the synaptophysin immunoreactivity was measured in this mask. The same mask was displaced away from the bulb, and the background intensity was measured and subtracted from the first measurement to obtain a semiquantitative estimate of synaptophysin contents in bulbs near and away from synapses.

To identify the cells that are associated with bulb-tipped axons, we stained with a polyclonal antibody for S100 (Dako, Carpinteria, CA). Around the bulb-tipped axons, S100-positive cells were regu-

larly seen, indicating that the cells adjacent to bulbs are Schwann cells.

Iontophoretic Labeling

Under pentobarbital anesthesia, sternomastoid muscles from P1–P10 mice were located and labeled with 5 μg/mL Alexa 488-conjugated α-bungarotoxin (Molecular Probes) to stain acetylcholine receptors as a guide for iontophoretic labeling of motor axons. Animals were fixed by transcardial perfusion of 2.5% glutaraldehyde and 2.0% paraformaldehyde in sodium cacodylate buffer (pH 7.4) containing Ca^{2+} (2 mM) and Mg^{2+} (4 mM). Although fixation with glutaraldehyde resulted in a large background autofluorescence, endplates could still be easily located. Motor neurons were labeled by iontophoretic application of 1,1′-dioctadecyl-3,3,3′,3′-tetramethylindocarbocyanine (DiI; Molecular Probes). A 1.0% solution of DiI dissolved in 100% methylene chloride was loaded into a 5–10 MΩ pipette with a chlorided silver wire serving as internal electrode. Small DiI crystals formed at the tip of the pipette when electrical pulses (200 ms, 1–10 V, 1 Hz; SD9 Stimulator; Grass Instruments, West Warwick, RI) were passed between electrode and ground. This small crystal was then deposited at the edge of an endplate after slightly penetrating the cell membrane of the muscle fiber and nerve terminals. Through diffusion of DiI within the axolemma, terminals of a motor unit were selectively labeled. Neuromuscular junctions, which belonged to this motor unit but were only partially covered by the labeled axon (and thus also innervated by an unlabeled axon), were chosen for reconstruction.

Confocal Imaging and Photoconversion

Neuromuscular junctions were imaged with a confocal microscope (BioRad MRC-1024) using a 60×, 0.9 NA water objective lens. A zoom factor of 2.5× was used to obtain maximum resolution. The confocal pinhole was optimized to remove background autofluorescence yet still collect sufficient light. Junctions were typically imaged only once so as not to bleach the fluorophore prior to photoconversion.

After confocal imaging, the entire preparation was bathed for 30 min in an oxygenated solution of diaminobenzidine (DAB; 5.0 mg/ml; Sigma) kept on ice. After a fresh change of cold, oxygenated DAB solution, the junction of interest was photoconverted by exciting DiI near its excitation wavelength for ~20 min with a 40×, 0.75 NA water immersion lens until a reddish-brown precipitate replaced the DiI fluorescence. At the electron microscopic level, the photoconversion reaction product was uniform and filled the cell rather than only being trapped in the axolemma. This is perhaps due to the fact that we penetrated the axolemma during deposition of the DiI crystal, thereby allowing the dye to diffuse between various lipid components inside the cell. The original DiI crystal was also photoconverted to aid in locating the junction of interest during thick sectioning as well as in the electron microscope.

Electron Microscopy

The muscle was prepared for plastic embedding by first trimming the muscle with a razor blade to a small region containing the photoconverted crystal and endplate. The tissue block was stained in 1.0% osmium-ferrocyanide for 30 min followed by 2.0% aqueous uranyl acetate. Following two exchanges of 0.1 M sodium cacodylate buffer, the tissue block was dehydrated in ascending ethanol solutions followed by two exchanges in 100% propylene oxide. Tissue blocks were infiltrated overnight with Araldite/Embed812 (Electron Microscopy Sciences, Hatfield, PA).

Tissue blocks were sectioned (1.0 μm) with glass knives until the photoconverted crystal was located. Serial ultrathin sections (60 nm) were then cut with a diamond knife (Diatome, Biel, Switzerland), placed on formvar-coated slot grids, and placed in a numbered grid box. Sections were then counterstained with 2.0% aqueous uranyl acetate for 30 min and Reynold's lead citrate for 30 min. Following staining, grids were coated with a thin carbon film with an Edwards coating (Edwards 520) system to add stability to the sections under the electron beam. Sections were then viewed at 80 KV using a JEOL 100CX electron microscope. A calibration grid was also photographed along with sections to aid in quantitative measurements. Section thickness was estimated as an average of measurements obtained with both the minimal fold method and the cylindrical diameters method (Fiala and Harris, 2001)

EM Reconstruction and Analysis

Electron micrographs were captured on film at 6700× and digitized with a scanner (Epson 1640SU; Long Beach, CA) at a resolution of 600 dpi, montaged (Adobe Photoshop), and then imported into an alignment and reconstruction software package (SEM Align and Trace) developed by Kristen Harris and John Fiala (available at Synapse Web [http://synapses.mcg.edu]). Briefly, each section is microaligned to an adjacent section either manually or by using fiduciary markers between the two sections until there is no systematic rotation between the two sections. Following alignment of the entire series, surface contours were manually traced. Surface contours were joined and rendered in three dimensions to generate a surface reconstruction of the desired object. Quantitative measurements (volume, surface area, object counts) were generated by the Trace software from surface contour data. Objects that were smaller than the section thickness (vesicles) were corrected for section thickness using the Abercrombie method for cell counting (Purves and Lichtman, 1985). Schwann cells were identified in electron micrographs as cells bounded by a basal lamina that sheathed preterminal axons or axon terminals.

Acknowledgments

The authors wish to thank Joshua Sanes for providing XFP mice; Judy Tollett for animal husbandry; Martin Kerschensteiner for valuable suggestions and critical reading of the manuscript; and the Indiana Center for Biological Microscopy. This work was supported by grants from the NIH (J.W.L.). D.L.B. was supported by a grant from the NIH and Muscular Dystrophy Association. T.M. was supported by an Emmy Noether Fellowship of the Deutsche Forschungsgemeinschaft.

Received: June 23, 2004
Revised: September 13, 2004
Accepted: October 6, 2004
Published: November 17, 2004

References

Awasaki, T., and Ito, K. (2004). Engulfing action of glial cells is required for programmed axon pruning during *Drosophila* metamorphosis. Curr. Biol. *14*, 668–677.

Balice-Gordon, R.J., and Lichtman, J.W. (1990). In vivo visualization of the growth of pre- and postsynaptic elements of neuromuscular junctions in the mouse. J. Neurosci. *10*, 894–908.

Balice-Gordon, R.J., Chua, C.K., Nelson, C.C., and Lichtman, J.W. (1993). Gradual loss of synaptic cartels precedes axon withdrawal at developing neuromuscular junctions. Neuron *11*, 801–815.

Bixby, J.L. (1981). Ultrastructural observations on synapse elimination in neonatal rabbit skeletal muscle. J. Neurocytol. *10*, 81–100.

Broadie, K. (2004). Axon pruning: an active role for glial cells. Curr. Biol. *14*, R302–R304.

Brown, M.C., Jansen, J.K., and Van Essen, D. (1976). Polyneuronal innervation of skeletal muscle in new-born rats and its elimination during maturation. J. Physiol. *261*, 387–422.

Chen, C., and Regehr, W.G. (2000). Developmental remodeling of the retinogeniculate synapse. Neuron *28*, 955–966.

Colman, H., Nabekura, J., and Lichtman, J.W. (1997). Alterations in synaptic strength preceding axon withdrawal. Science *275*, 356–361.

Conradt, B. (2002). With a little help from your friends: cells don't die alone. Nat. Cell Biol. *4*, E139–E143.

Dennis, M.J., and Miledi, R. (1974). Electrically induced release of acetylcholine from denervated Schwann cells. J. Physiol. *237*, 431–452.

Denzer, K., Kleijmeer, M.J., Heijnen, H.F., Stoorvogel, W., and Geuze, H.J. (2000). Exosome: from internal vesicle of the multivesicular body to intercellular signaling device. J. Cell Sci. *113*, 3365–3374.

Eckenhoff, M.F., and Pysh, J.J. (1979). Double-walled coated vesicle formation: evidence for massive and transient conjugate internalization of plasma membranes during cerebellar development. J. Neurocytol. *8*, 623–638.

Feng, G., Mellor, R.H., Bernstein, M., Keller-Peck, C., Nguyen, Q.T., Wallace, M., Nerbonne, J.M., Lichtman, J.W., and Sanes, J.R. (2000). Imaging neuronal subsets in transgenic mice expressing multiple spectral variants of GFP. Neuron *28*, 41–51.

Fiala, J.C., and Harris, K.M. (2001). Cylindrical diameters method for calibrating section thickness in serial electron microscopy. J. Microsc. *202*, 468–472.

Gan, W.B., and Lichtman, J.W. (1998). Synaptic segregation at the developing neuromuscular junction. Science *282*, 1508–1511.

Gan, W.B., Bishop, D.L., Turney, S.G., and Lichtman, J.W. (1999). Vital imaging and ultrastructural analysis of individual axon terminals labeled by iontophoretic application of lipophilic dye. J. Neurosci. Methods *93*, 13–20.

Gillingwater, T.H., and Ribchester, R.R. (2001). Compartmental neurodegeneration and synaptic plasticity in the Wld(s) mutant mouse. J. Physiol. *534*, 627–639.

Gillingwater, T.H., Ingham, C.A., Coleman, M.P., and Ribchester, R.R. (2003). Ultrastructural correlates of synapse withdrawal at axotomized neuromuscular junctions in mutant and transgenic mice expressing the Wld gene. J. Anat. *203*, 265–276.

Greco, V., Hannus, M., and Eaton, S. (2001). Argosomes: a potential vehicle for the spread of morphogens through epithelia. Cell *106*, 633–645.

He, Y., Yu, W., and Baas, P.W. (2002). Microtubule reconfiguration during axonal retraction induced by nitric oxide. J. Neurosci. *22*, 5982–5991.

Henson, P.M., Bratton, D.L., and Fadok, V.A. (2001). Apoptotic cell removal. Curr. Biol. *11*, R795–R805.

Hirata, K., and Kawabuchi, M. (2002). Myelin phagocytosis by macrophages and nonmacrophages during Wallerian degeneration. Microsc. Res. Tech. *57*, 541–547.

Hirokawa, N., Noda, Y., and Okada, Y. (1998). Kinesin and dynein superfamily proteins in organelle transport and cell division. Curr. Opin. Cell Biol. *10*, 60–73.

Italiano, J.E., Jr., and Shivdasani, R.A. (2003). Megakaryocytes and beyond: the birth of platelets. J. Thromb. Haemost. *1*, 1174–1182.

Keller-Peck, C.R., Walsh, M.K., Gan, W.B., Feng, G., Sanes, J.R., and Lichtman, J.W. (2001). Asynchronous synapse elimination in neonatal motor units: studies using GFP transgenic mice. Neuron *31*, 381–394.

Korneliussen, H., and Jansen, J.K. (1976). Morphological aspects of the elimination of polyneuronal innervation of skeletal muscle fibres in newborn rats. J. Neurocytol. *5*, 591–604.

Lichtman, J.W. (1977). The reorganization of synaptic connexions in the rat submandibular ganglion during post-natal development. J. Physiol. *273*, 155–177.

Lichtman, J.W., and Purves, D. (1980). The elimination of redundant preganglionic innervation to hamster sympathetic ganglion cells in early post-natal life. J. Physiol. *301*, 213–228.

Lin, W., Sanchez, H.B., Deerinck, T., Morris, J.K., Ellisman, M., and Lee, K.F. (2000). Aberrant development of motor axons and neuromuscular synapses in erbB2-deficient mice. Proc. Natl. Acad. Sci. USA *97*, 1299–1304.

Lohof, A.M., Delhaye-Bouchaud, N., and Mariani, J. (1996). Synapse elimination in the central nervous system: functional significance and cellular mechanisms. Rev. Neurosci. *7*, 85–101.

Marston, D.J., Dickinson, S., and Nobes, C.D. (2003). Rac-dependent trans-endocytosis of ephrinBs regulates Eph-ephrin contact repulsion. Nat. Cell Biol. *5*, 879–888.

Martinez-Lorenzo, M.J., Anel, A., Gamen, S., Monleón, I., Lasierra, P., Larrad, L., Pineiro, A., Alava, M.A., and Naval, J. (1999). Activated human T cells release bioactive Fas ligand and APO2 ligand in microvesicles. J. Immunol. *163*, 1274–1281.

Miledi, R., and Slater, C.R. (1968). Electrophysiology and electron-microscopy of rat neuromuscular junctions after nerve degeneration. Proc. R. Soc. Lond. B. Biol. Sci. *169*, 289–306.

Nakao, J., Shinoda, J., Nakai, Y., Murase, S., and Uyemura, K. (1997). Apoptosis regulates the number of Schwann cells at the premyelinating stage. J. Neurochem. *68*, 1853–1862.

Nedergaard, M., Ransom, B., and Goldman, S.A. (2003). New roles for astrocytes: redefining the functional architecture of the brain. Trends Neurosci. *26*, 523–530.

Parson, S.H., Ribchester, R.R., Davie, N., Gandhi, N.P., Malik, R.Q., Gillingwater, T.H., and Thomson, D. (2004). Axotomy-dependent and -independent synapse elimination in organ cultures of Wld(s) mutant mouse skeletal muscle. J. Neurosci. Res. *76*, 64–75.

Purves, D., and Lichtman, J.W. (1985). Principles of Neural Development, First Edition (Sunderland, MA: Sinauer Associates).

Reddy, L.V., Koirala, S., Sugiura, Y., Herrera, A.A., and Ko, C.P. (2003). Glial cells maintain synaptic structure and function and promote development of the neuromuscular junction in vivo. Neuron *40*, 563–580.

Redfern, P.A. (1970). Neuromuscular transmission in new-born rats. J. Physiol. *209*, 701–709.

Ribbeck, K., and Gorlich, D. (2001). Kinetic analysis of translocation through nuclear pore complexes. EMBO J. *20*, 1320–1330.

Riley, D.A. (1981). Ultrastructural evidence for axon retraction during the spontaneous elimination of polyneuronal innervation of the rat soleus muscle. J. Neurocytol. *10*, 425–440.

Roos, J., Hummel, T., Ng, N., Klambt, C., and Davis, G.W. (2000). *Drosophila* Futsch regulates synaptic microtubule organization and is necessary for synaptic growth. Neuron *26*, 371–382.

Rosenthal, J.L., and Taraskevich, P.S. (1977). Reduction of multiaxonal innervation at the neuromuscular junction of the rat during development. J. Physiol. *270*, 299–310.

Spacek, J., and Harris, K.M. (2004). Trans-endocytosis via spinules in adult rat hippocampus. J. Neurosci. *24*, 4233–4241.

Trachtenberg, J.T., and Thompson, W.J. (1996). Schwann cell apoptosis at developing neuromuscular junctions is regulated by glial growth factor. Nature *379*, 174–177.

Walsh, M.K., and Lichtman, J.W. (2003). In vivo time-lapse imaging of synaptic takeover associated with naturally occurring synapse elimination. Neuron *37*, 67–73.

Watts, R.J., Hoopfer, E.D., and Luo, L. (2003). Axon pruning during *Drosophila* metamorphosis: evidence for local degeneration and requirement of the ubiquitin-proteasome system. Neuron *38*, 871–885.

Watts, R.J., Schuldiner, O., Perrino, J., Larsen, C., and Luo, L. (2004). Glia engulf degenerating axons during developmental axon pruning. Curr. Biol. *14*, 678–684.

Wekerle, H., Linington, C., Lassmann, H., and Meyermann, R. (1986). Cellular immune reactivity within the CNS. Trends Neurosci. *9*, 271–277.

Wyatt, R.M., and Balice-Gordon, R.J. (2003). Activity-dependent elimination of neuromuscular synapses. J. Neurocytol. *32*, 777–794.